Supplemental Information

RNAi screening reveals a large signaling network controlling the Golgi apparatus in human cells

Joanne Chia[1], Germaine Goh[1], Victor Racine[1], Susanne Ng[1], Pankaj Kumar[1] and Frederic Bard[1,2,*]

[1]Institute of Molecular and Cell Biology, 61 Biopolis Drive, Proteos, Singapore 138673

[2]National University of Singapore, 21 Lower Kent Ridge Road, Singapore 119077

Supplemental Table of Contents

SUPPLEMENTAL FIGURES

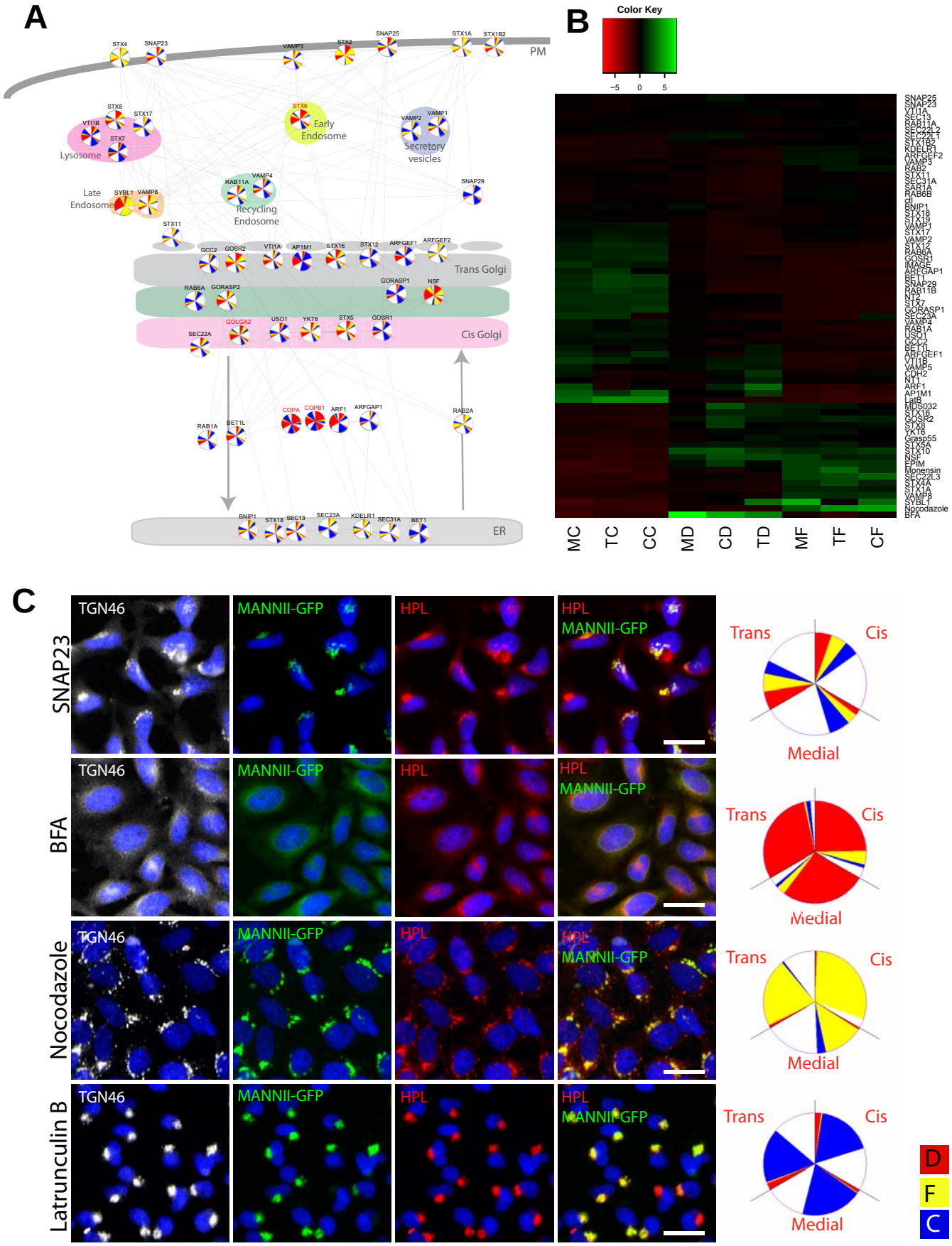

Figure S1

Figure S1. A pilot membrane trafficking screen identifies and quantifies three major Golgi phenotypes.

(A) A network of interactions of the 63 known regulators of membrane traffic tested in the pilot screen arranged in accordance with Cellular Component GO and literature review. Nodes with red names indicate genes that affect cell viability upon KD. (B) Heatmap of the phenotypic scores of the 63 membrane trafficking regulators. (C) Morphological signatures based on phenotypic scores reflect the extent of Golgi perturbation as highlighted by the completely diffused Golgi in Brefeldin A (BFA) treatment and a less extensively diffused Golgi in SNAP23 KD. Examples of extensively fragmented and condensed Golgi are reflected in nocodazole and latrunculin B treatments respectively. Bars: 30 μm.

A

Golgi compartment	Cis				Medial				Trans			
Phenotype	Diffuse	Fragmented	Condensed	Normal	Diffuse	Fragmented	Condensed	Normal	Diffuse	Fragmented	Condensed	Normal
Drug and siRNA treatments	BFA	Monensin	AP1M1	Control	BFA	IKBKE	AP1M1	Control	BFA	Monensin	CLK1	Control
		Nocodazole	CLK1			NSF	ARF1			Nocodazole	MKNK1	
		SEC22L3	MKNK1			Monensin	CLK1			ITPKB	GCK	
		ITPKB	GCK			Nocodazole	MKNK1			KHK	CDC2L2	
		SYBL1	CDC2L2			SYBL1	CDC2L2			DMPK	RIPK2	
		EPHA1	RIPK2			KHK	RIPK2			TSKS	MYO3A	
		TSKS	Latrunculin B			EPHA1	GAP43			STX4A	Latrunculin B	
		STX4A	MGC42105			EPHA1	SNAP47			MAPK12	MGC42105	
		MAPK12				TSKS	SRMS					
						STX4A	Latrunculin B					
						MAPK12	PKM2					
							MGC42105					

B

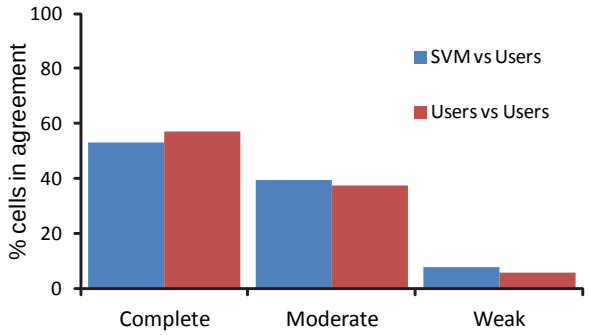

C

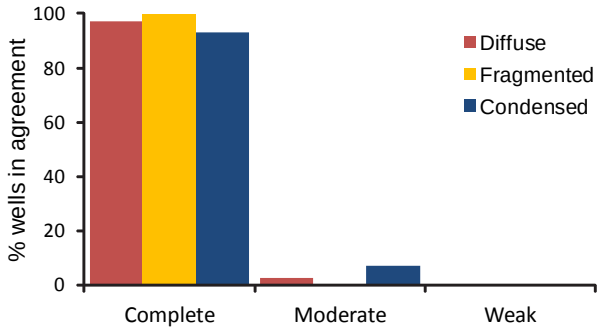

D

	Image Features	z-Score
Diffuse	Obj[2].surf	0.8435
	Obj[2].pctIntensity	0.7599
	Obj[1].peri	0.3297
	Obj[2].valMorpho	0.3162
	Obj[1].valMorpho	0.2831
Fragmented	Obj[1].nbSubstructures	0.577
	Obj[2].sigma.x	0.496
	Obj[2].sigma.y	0.4489
	Obj[2].peri	0.3841
	Obj[1].avgDistFromObjectsToSegCenter	0.3744
Condensed	Obj[2].sigma.y	0.2862
	Obj[1].nbSubstructures	0.286
	Obj[2].pctIntensity	0.233
	Obj[1].surf	0.2048
	Obj[2].surf	0.2044

E

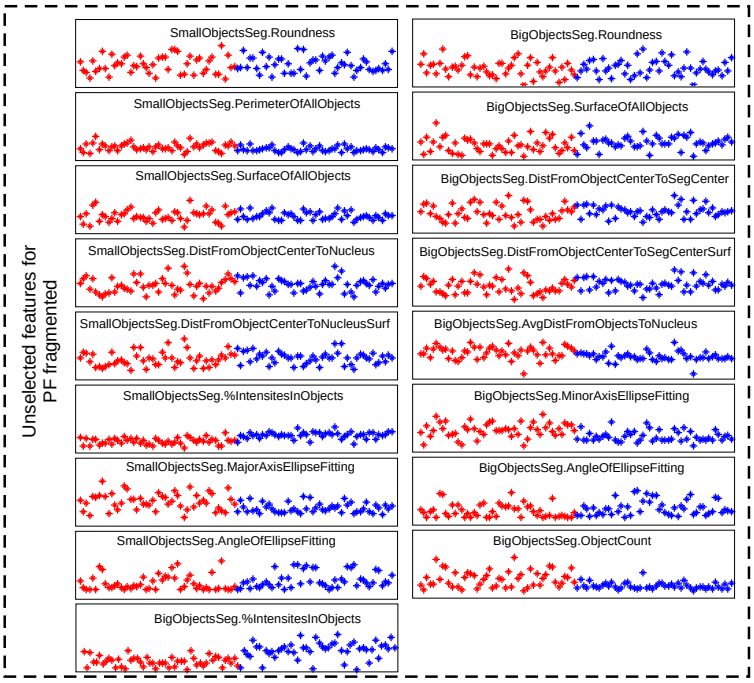

F

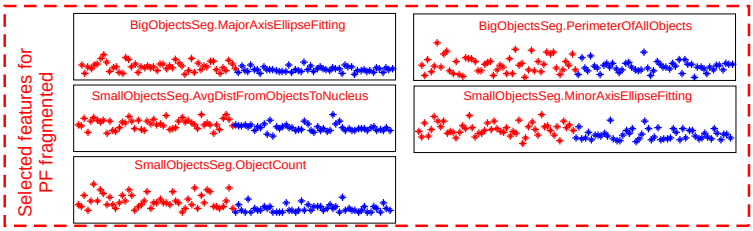

G

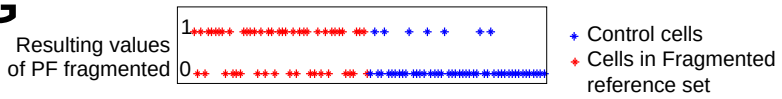

Figure S2

Figure S2. Support Vector Machine training using reference cells accurately describes Golgi phenotypes, consistent with visual inspection.

(A) Cells that were subjected to the listed drug (*blue)* and siRNA treatments were used to train the SVM to identify specific Golgi phenotypes in the three compartments. This list constitutes the "Reference morphological phenotypes" (Figure 1B and 2F). (B) Cellular validation of Golgi phenotypes by user compared to SVM. The percentage of cells for which the phenotype defined agrees between SVM and user (*Blue*), or between users (*red*) for each category "Complete", "Moderate" and "Weak". (C) Validation of predicted phenotypes at the well level. The percentage of wells for which each of the three Golgi phenotype defined agrees between user and SVM. (D) For each classifier, the 5 most discriminant image features were selected according to their z-scores to derive SVM functions that define phenotypic boundaries in this 5-dimensional space. Plots of unselected (E) and selected (F) raw image features of both control cells (*blue*) and cells that were predicted by the SVM with fragmented Golgi (*red*). Y axis indicates image feature scores. "BigobjectsSeg" and "SmallObjectsSeg" refer respectively to objects of roughly the size of a normal Golgi or large Golgi fragments and vesicles or small Golgi fragments (G) The 5 selected image features of the selected reference images were combined to generate the SVM for diffuse, fragmented (shown here) and condensed PF classification. The output is binary (1=fragmented or 0=not fragmented). The plot represents the PF classification of a group of control cells and cells from the fragmented reference set, demonstrating that the PF is much better at describing cellular phenotype than any of the individual image features. The cells from the

reference set that are not classified as fragmented reflect the phenotypic heterogeneity of cell populations.

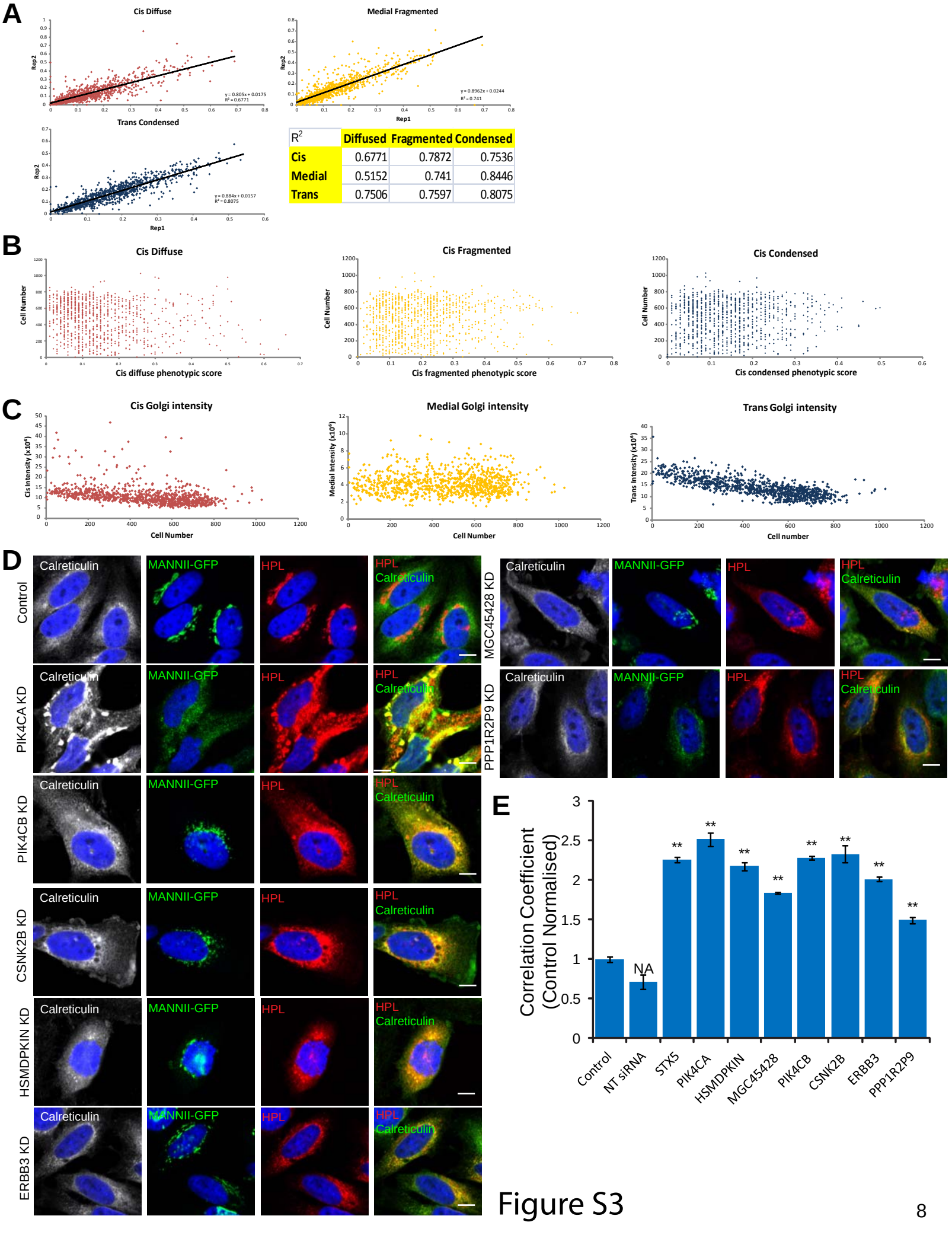

R^2	Diffused	Fragmented	Condensed
Cis	0.6771	0.7872	0.7536
Medial	0.5152	0.741	0.8446
Trans	0.7506	0.7597	0.8075

Figure S3

Figure S3. Phenotypic scores are reproducible across replicates and independent of cell number.

(A) Scatter plots demonstrating reproducibility in the phenotypic scores between the two screen replicates. (B) Plots of total cell count versus phenotypic scores reveal absence of correlation between cell number and Golgi phenotype. (C) Plots comparing intensities of Golgi compartments with cell count show absence of correlation. (D) Genes that show a cis diffuse Golgi and secretion defects upon depletion show extensive colocalization between cis Golgi marker HPL and ER marker calreticulin. Images were acquired with 60x magnification. Scale bar: 10 μm. (E) Colocalization between the cis Golgi and ER markers was measured using Pearson's correlation coefficient of the staining intensities of the two markers. Cells were analysed using Metaexpress Translocation-Enhanced analysis module. Values on graphs indicate the mean ± SEM. **$p<0.0001$, *$p<0.05$ by two-tailed unpaired t- test, relative to untransfected control cells.

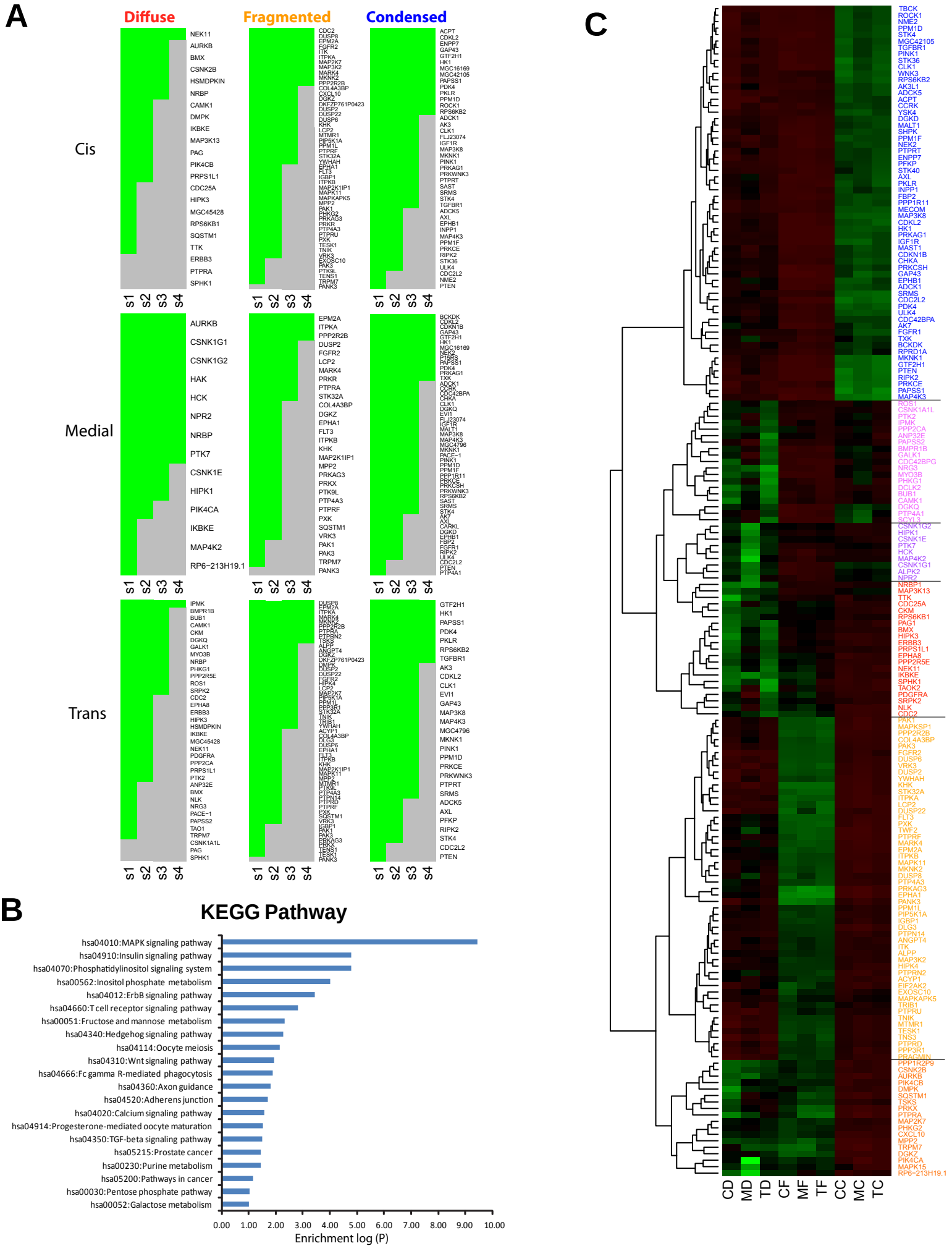
A
Diffuse
Fragmented
Condensed
Cis
Medial
Trans
s1
s2
s3
s4
B
KEGG Pathway
hsa04010:MAPK signaling pathway
hsa04910:Insulin signaling pathway
hsa04070:Phosphatidylinositol signaling system
hsa00562:Inositol phosphate metabolism
hsa04012:ErbB signaling pathway
hsa04660:T cell receptor signaling pathway
hsa00051:Fructose and mannose metabolism
hsa04340:Hedgehog signaling pathway
hsa04114:Oocyte meiosis
hsa04310:Wnt signaling pathway
hsa04666:Fc gamma R-mediated phagocytosis
hsa04360:Axon guidance
hsa04520:Adherens junction
hsa04020:Calcium signaling pathway
hsa04914:Progesterone-mediated oocyte maturation
hsa04350:TGF-beta signaling pathway
hsa05215:Prostate cancer
hsa00230:Purine metabolism
hsa05200:Pathways in cancer
hsa00030:Pentose phosphate pathway
hsa00052:Galactose metabolism
0.00
1.00
2.00
3.00
4.00
5.00
6.00
7.00
8.00
9.00
10.00
Enrichment log (P)
C
CD
MD
TD
CF
MF
TF
CC
MC
TC

Figure S4

Figure S4. Most of the primary hit phenotypes are reproducible using deconvoluted siRNAs and demonstrate enrichment in some signaling pathways.

(A) Hit validation using deconvoluted siRNA pools. Golgi phenotypic scoring was performed with 4 individual duplex siRNAs from the pool for each of the 181 genes. For each Golgi phenotype, each set of four duplexes was ranked based on the number of duplexes that have a score above the threshold. A gene was validated if at least two unique siRNAs gave a score above the threshold. (B) Enrichment studies of hit genes based on biological pathway annotation in KEGG database. (C) Enlarged version of Figure 3C.

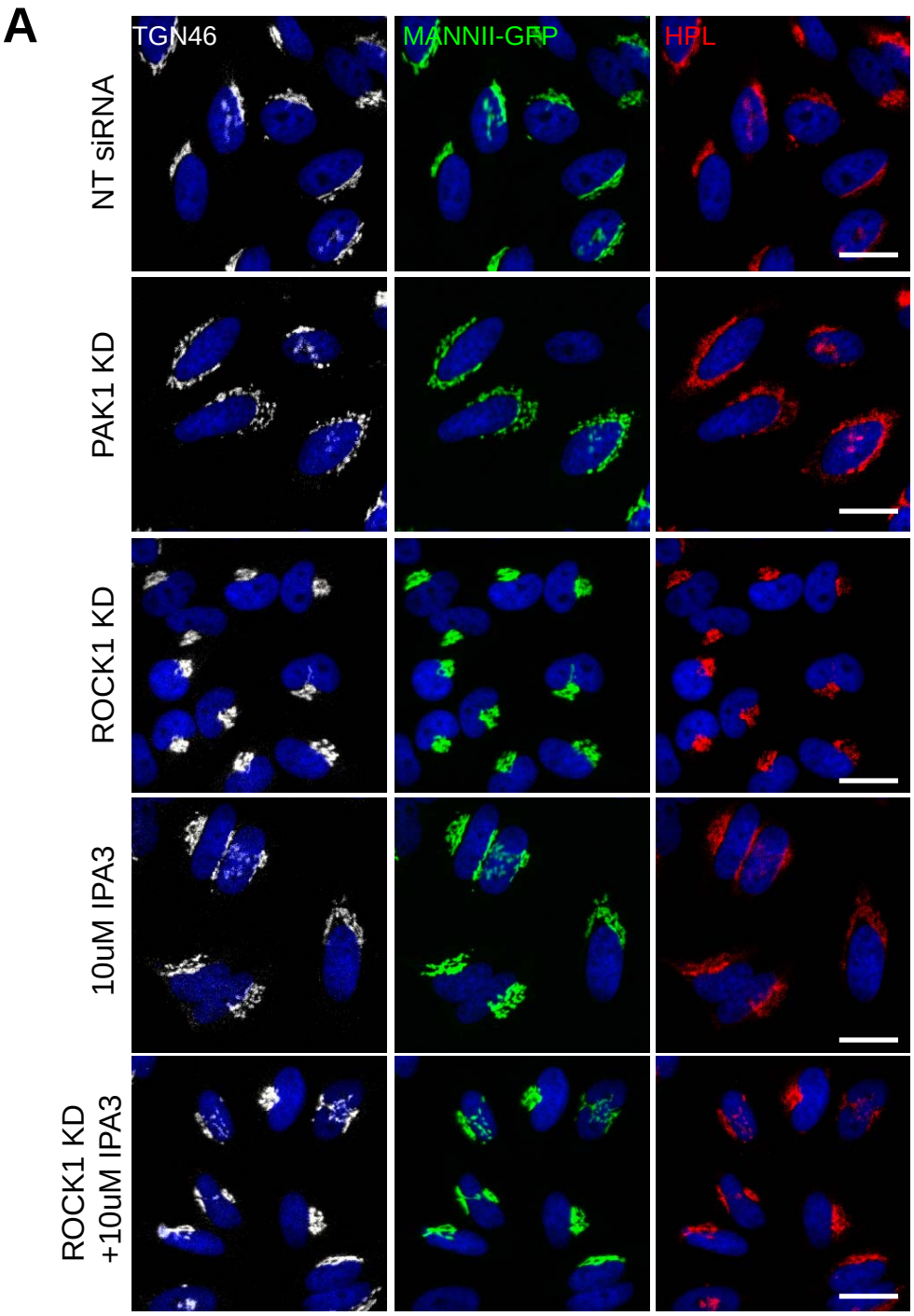
A
TGN46
MANNII-GFP
HPL
NT siRNA
PAK1 KD
ROCK1 KD
10uM IPA3
ROCK1 KD
+10uM IPA3

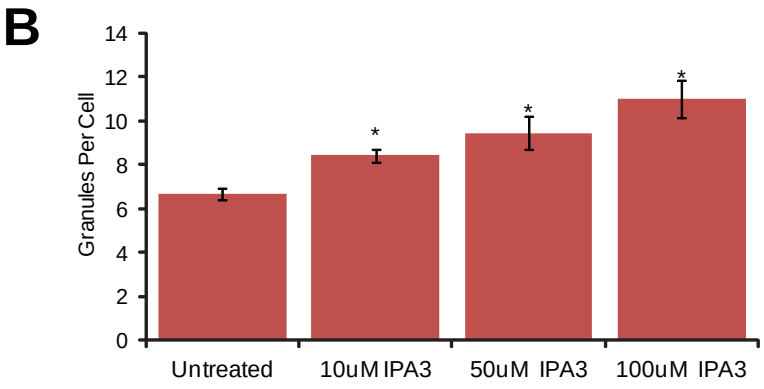
B
Granules Per Cell
0
2
4
6
8
10
12
14
Untreated
10uM IPA3
50uM IPA3
100uM IPA3

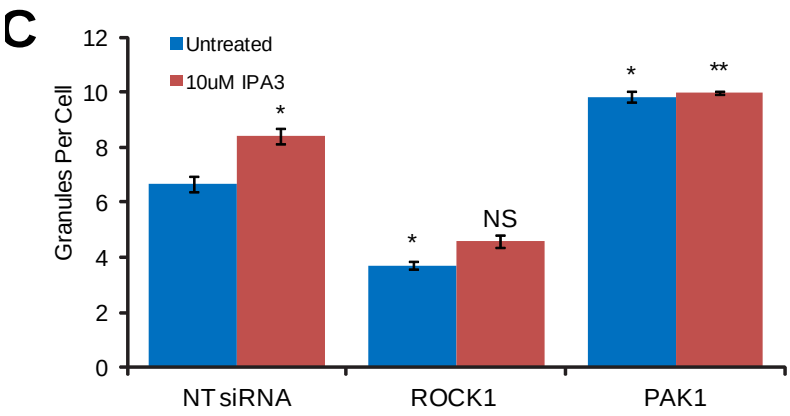
C
Untreated
10uM IPA3
Granules Per Cell
0
2
4
6
8
10
12
NS
NT siRNA
ROCK1
PAK1

Figure S5

Figure S5. Actomyosin regulators ROCK1 and PAK1 exhibit antagonistic effects on Golgi structure.

(A) Treatment of cells with 10μM of PAK inhibitor IPA3 recapitulated the fragmented Golgi phenotype in PAK1 depletion. ROCK1 depleted cells treated with IPA3 reverted the condensed Golgi phenotype to normal. (B) Quantification of the number of granules per cell of cells treated for 6 hours with different IPA3 concentrations. (C) Quantification of the number of granules per cell with (red bars) and without (blue bars) treatment of 10μM IPA3 on siRNA depleted cells. Values on graphs indicate the mean ± SEM. **$p<0.0001$, *$p<0.05$ by two-tailed unpaired t-test, relative to non- targeting siRNA treated control cells.

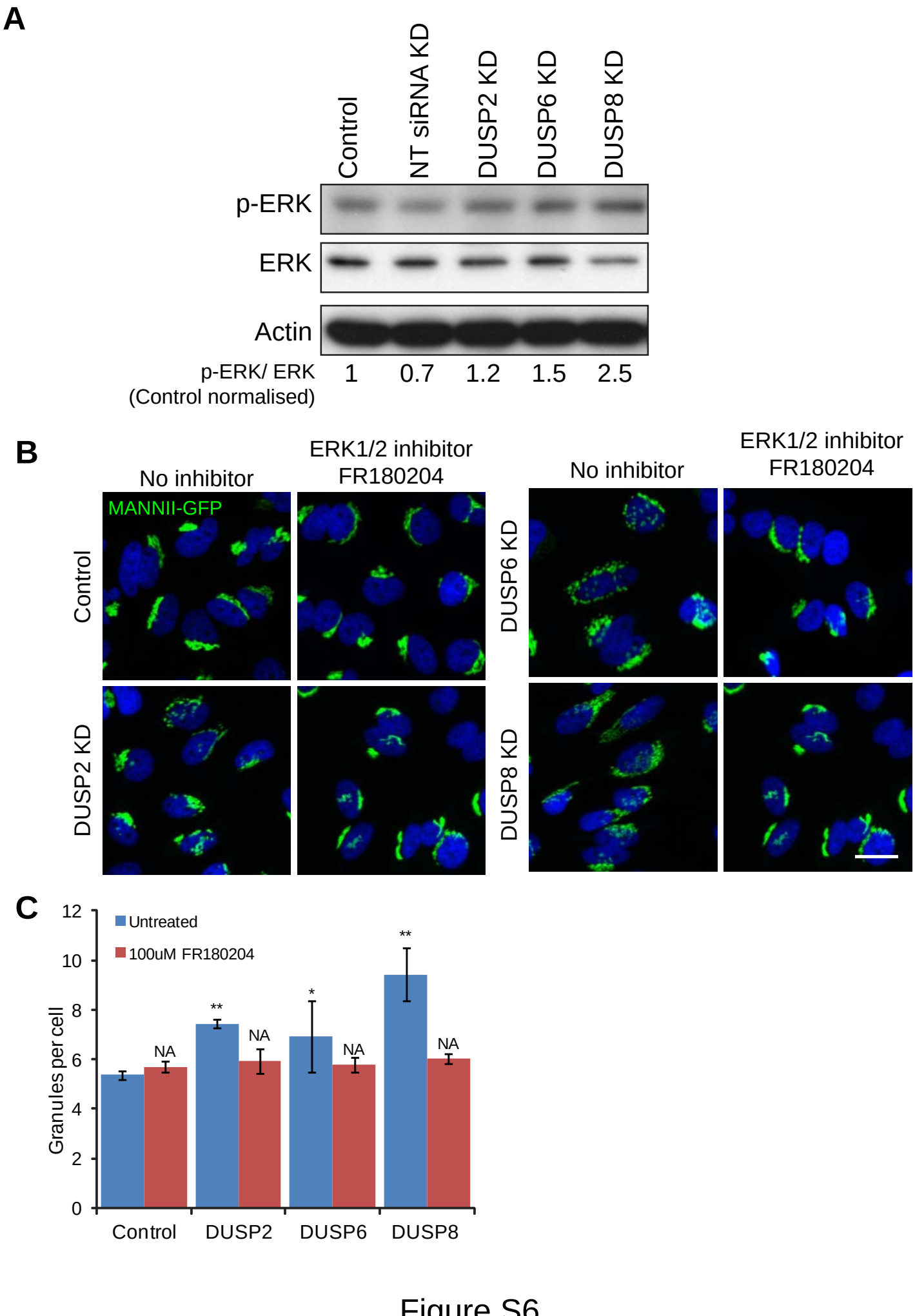
A
Control
NT siRNA KD
DUSP2 KD
DUSP6 KD
DUSP8 KD
p-ERK
ERK
Actin
p-ERK/ ERK
(Control normalised)
1
0.7
1.2
1.5
2.5
B
No inhibitor
ERK1/2 inhibitor
FR180204
MANNII-GFP
Control
DUSP2 KD
DUSP6 KD
DUSP8 KD
C
Untreated
100uM FR180204
Granules per cell
NA
**
*
Control
DUSP2
DUSP6
DUSP8

Figure S6

Figure S6. Golgi fragmentation by depletion of DUSPs requires ERK1/2 activation.

(A) Western blot analysis of phosphorylated and total ERK levels in the siRNA KD of DUSP2, 6 and 8. Phospho-ERK/total-ERK levels normalised to control cells were quantified using ImageJ software and indicated below the respective lanes. (B) Treatment of DUSP-depleted cells with 100 μM ERK1/2 inhibitor FR180204 for 6 hours rescues the fragmented Golgi phenotype. Scale bar: 10 μm. (C) Quantification of the number of granules per cell of cells with (red bars) and without (blue bars) drug treatments. Values on graphs indicate the mean ± SEM. **p<0.0001, *p<0.05 by two-tailed unpaired t-test, relative to untreated control cells.

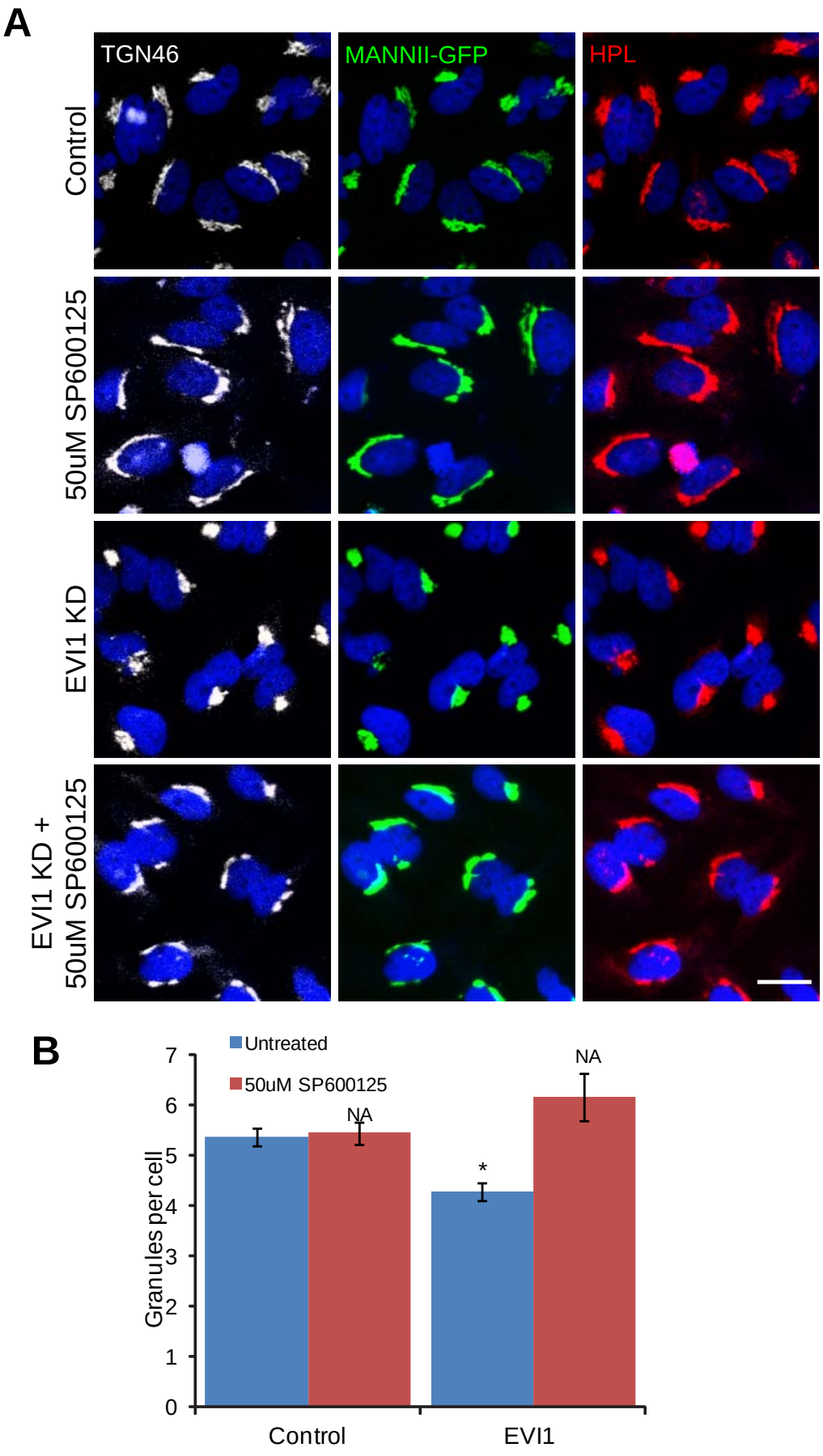
A
TGN46
MANNII-GFP
HPL
Control
50uM SP600125
EVI1 KD
EVI1 KD +
50uM SP600125
B
Untreated
50uM SP600125
Granules per cell
0
1
2
3
4
5
6
7
NA
NA
*
Control
EVI1

Figure S7

Figure S7. Condensed Golgi phenotype from MECOM depletion is due to JNK activation.

(A) The condensed Golgi phenotype in MECOM depleted cells is rescued back to normal after treatment with 50 μM of JNK inhibitor SP600125 for 6 hours. (B) Quantification of the number of granules per cell with (red bars) and without (blue bars) drug treatment. Values on graphs indicate the mean ± SEM. **p<0.0001, *p<0.05 by two-tailed unpaired t-test, relative to untreated control cells.

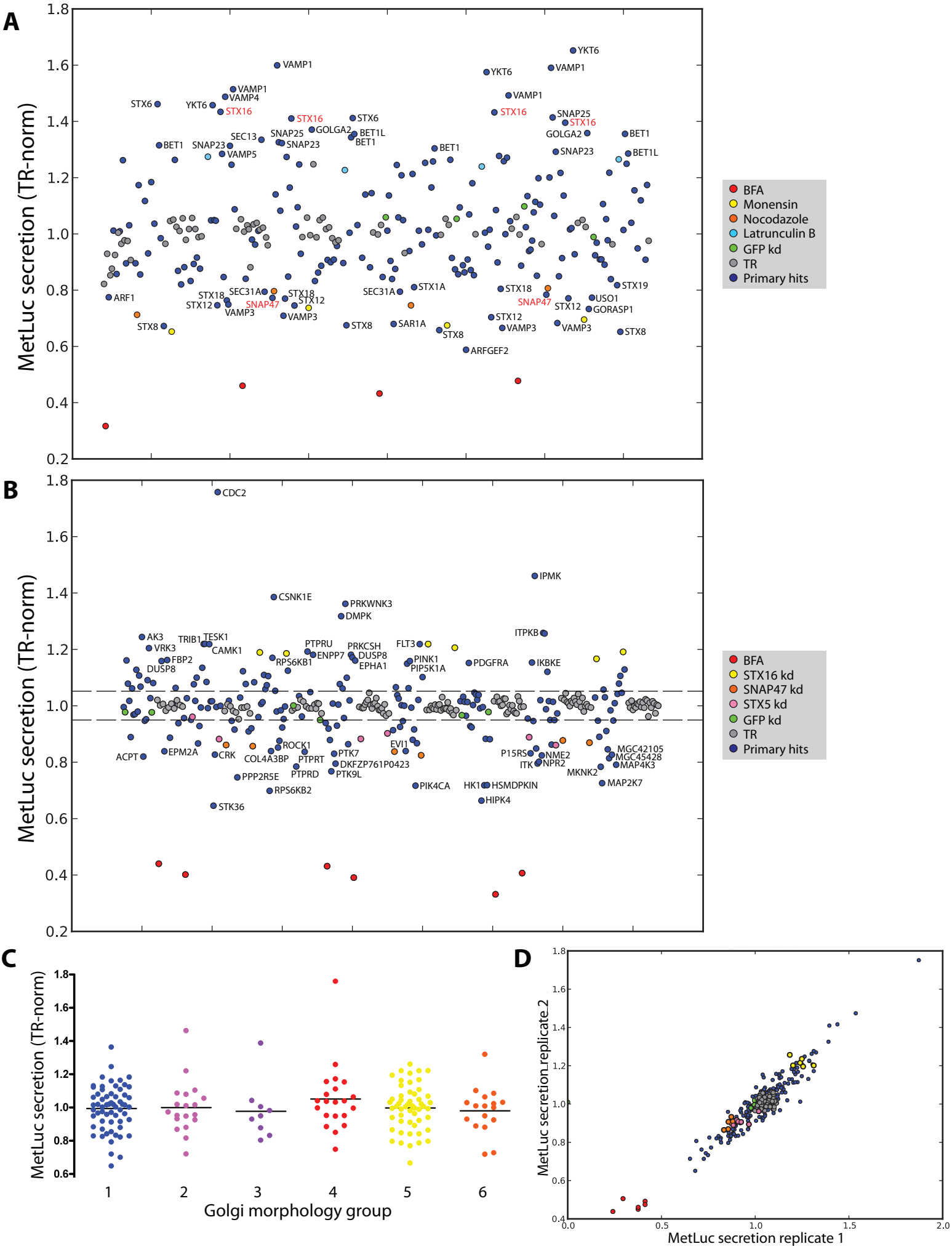
A
MetLuc secretion (TR-norm)
BFA
Monensin
Nocodazole
Latrunculin B
GFP kd
TR
Primary hits
B
MetLuc secretion (TR-norm)
BFA
STX16 kd
SNAP47 kd
STX5 kd
GFP kd
TR
Primary hits
C
MetLuc secretion (TR-norm)
Golgi morphology group
D
MetLuc secretion replicate 2
MetLuc secretion replicate 1

Figure S8

Figure S8. Depletion of 111 Golgi organization regulators results in significant changes in secretion.

Met-Luc secretion (log of luciferin signal per cell, normalized to that of transfection reagent-treated control (TR) wells) of (A) genes in the pilot screen and (B) the primary Golgi morphology hit genes. Control wells are indicated as in the legend. Some genes on the extremes are labeled. Dashed lines in (B) indicate the cutoff values for significant secretion changes. (C) Met-Luc secretion of the primary hit genes, grouped according to the 6 Golgi morphology groups, indicating no significant correlation between Golgi morphology and constitutive secretion of Met-Luc. Lines indicate the group mean. (D) Plot of the Met-Luc secretion values of the primary hit genes for the two replicate experiments. Data points are color-coded as in (B).

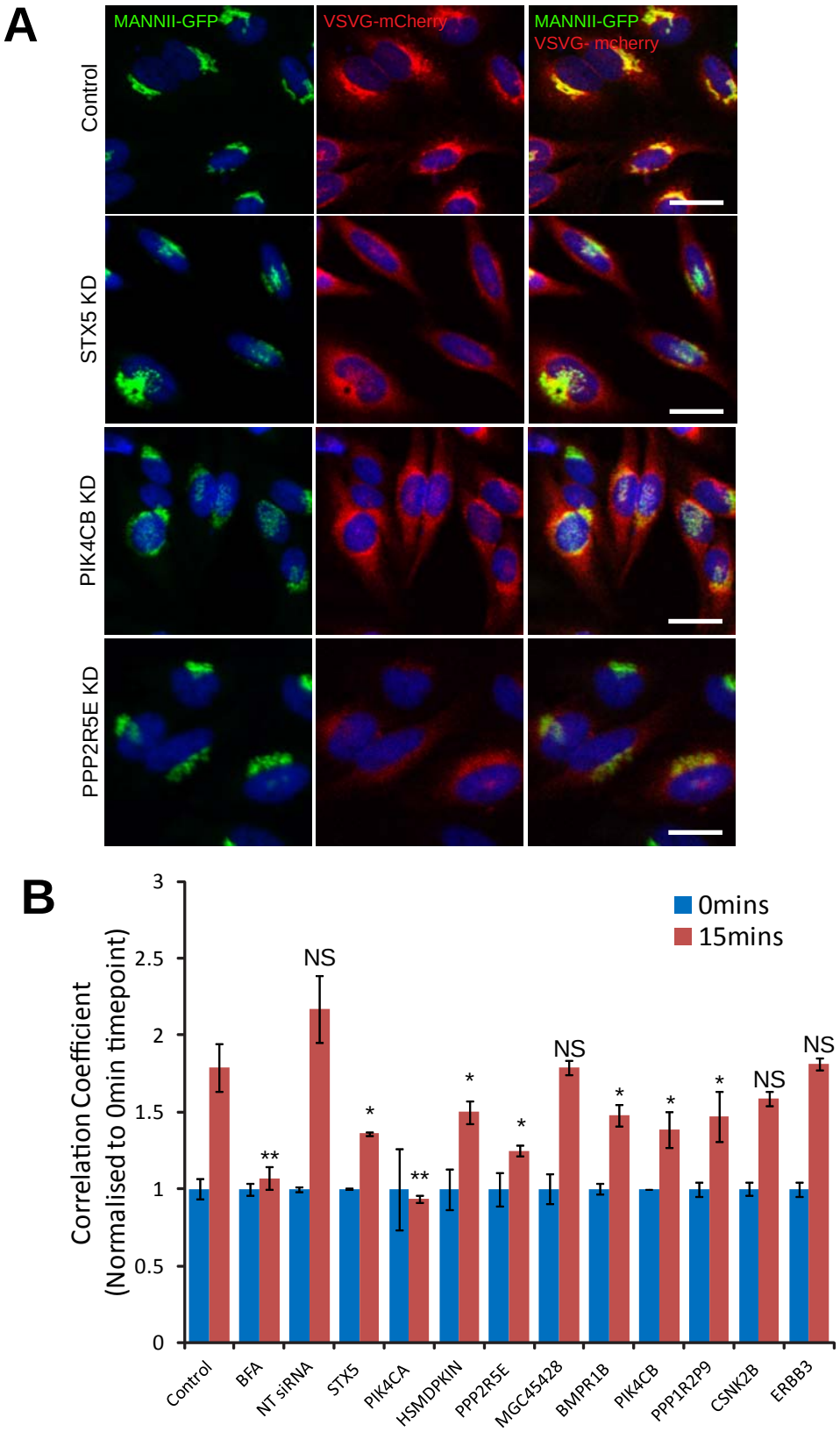
A
MANNII-GFP
VSVG-mCherry
MANNII-GFP
VSVG- mcherry
Control
STX5 KD
PIK4CB KD
PPP2R5E KD
B
0mins
15mins
Correlation Coefficient
(Normalised to 0min timepoint)
3
2.5
2
1.5
1
0.5
0
NS
**
*
**
*
*
NS
*
*
NS
NS
Control
BFA
NT siRNA
STX5
PIK4CA
HSMDPKIN
PPP2R5E
MGC45428
BMPR1B
PIK4CB
PPP1R2P9
CSNK2B
ERBB3

Figure S9

Figure S9. Depletion of genes that show cis diffuse Golgi exhibit ER to Golgi trafficking defects with VSVG.

(A) ER-Golgi trafficking of VSVG-tsO45-mcherry is impaired upon depletion of most genes that display both cis diffuse Golgi and reduced Met-Luc secretion phenotypes.

(B) VSVG appearance at the Golgi after 15 min was quantified by Pearson's correlation coefficient of the staining intensities of the Golgi marker MannII-GFP and VSVG (red bars). Plots show correlation coefficients normalised to their respective controls at 0 min (blue bars). Cells were analysed using Metaexpress Translocation-Enhanced analysis module. Values on graphs indicate the mean ± SEM. **p<0.0001, *p<0.05 by two-tailed unpaired t-test, relative to untransfected control cells at 15 min.

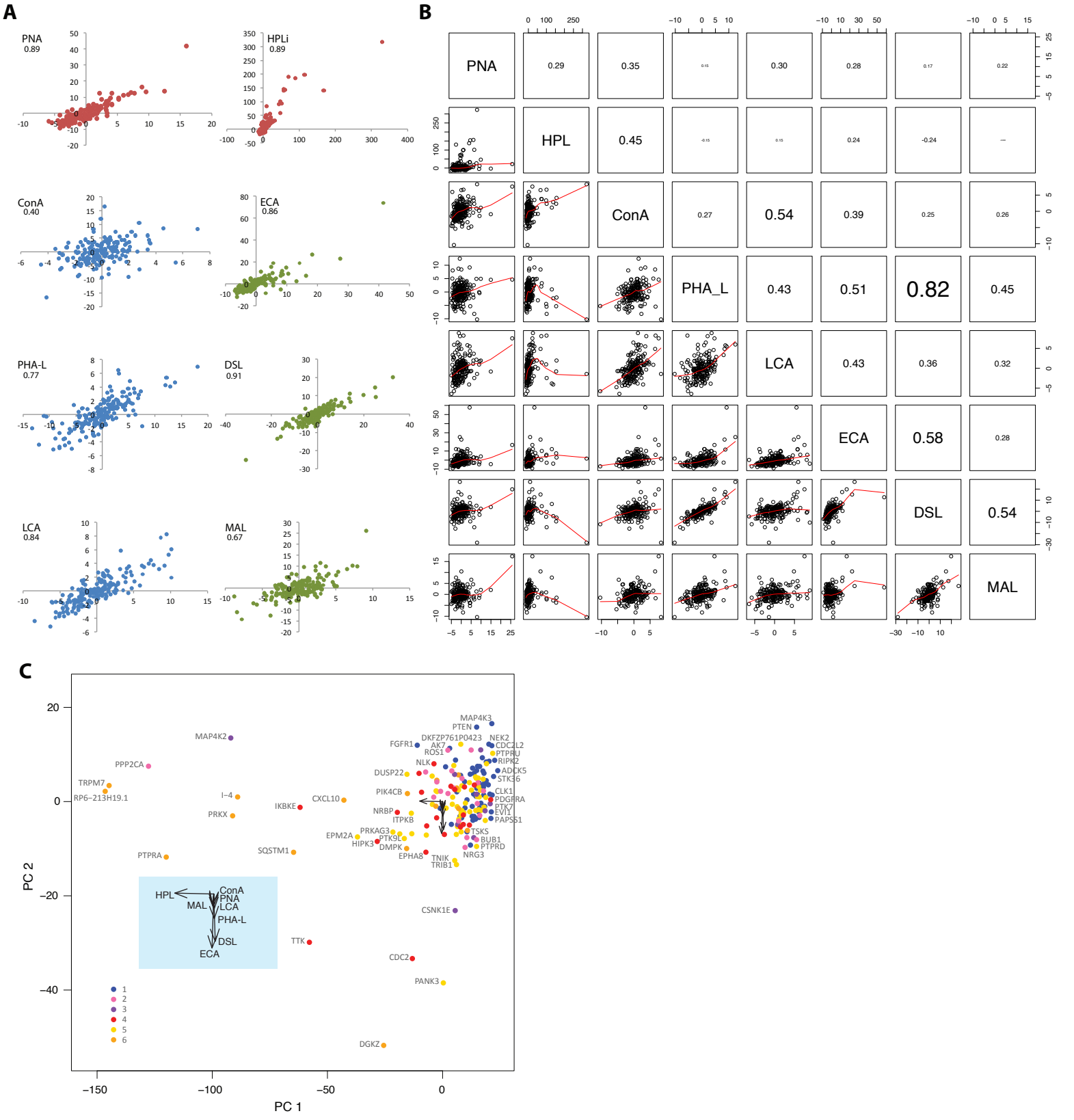
A
PNA
0.89
HPLi
0.89
ConA
0.40
ECA
0.86
PHA-L
0.77
DSL
0.91
LCA
0.84
MAL
0.67
B
PNA
0.29
0.35
0.30
0.28
0.22
HPL
0.45
0.24
ConA
0.27
0.54
0.39
0.25
0.26
PHA_L
0.43
0.51
0.82
0.45
LCA
0.43
0.36
0.32
ECA
0.58
0.28
DSL
0.54
MAL
C
PC 1
PC 2
HPL
MAL
ConA
PNA
LCA
PHA-L
DSL
ECA
MAP4K3
PTEN
MAP4K2
DKFZP761P0423
NEK2
FGFR1
AK7
CDC2L2
ROS1
PTPRU
PPP2CA
NLK
RIPK2
DUSP22
ADCK5
TRPM7
STK36
PIK4CB
CLK1
RP6-213H19.1
I-4
CXCL10
PDGFRA
IKBKE
PTK7
PRKX
NRBP
EVI1
ITPKB
PAPSS1
PRKAG3
TSKS
EPM2A
PTK9L
BUB1
HIPK3
DMPK
PTPRD
PTPRA
EPHA8
NRG3
SQSTM1
TNIK
TRIB1
CSNK1E
TTK
CDC2
PANK3
DGKZ

Figure S10

Figure S10. Lectin signals are reproducible across replicates and generally independent of each other.

(A) Plots of normalized lectin signals for replicate experiments with each lectin, with one replicate on the x-axis and another replicate on the y-axis. Pearson correlation coefficients are indicated below the lectin names. (B) Plots of pairwise comparisons between the normalized lectin signals for different lectins. Squares on the bottom left of the diagonal are plots of the primary hit genes (*black*). Squares on the top right of the diagonal contain the Pearson correlation coefficients between paired lectins. (C) Principal Component Analysis plot of the 8 lectin scores for each hit gene illustrates the strong perturbations in HPL staining and its independence from the other lectins. Genes are color coded according to the 6 Golgi morphology groups as indicated. The strongest HPL hits tend to have diffuse or fragmented phenotypes. *Inset*: Magnified view of the Eigen vectors of the lectins.

SUPPLEMENTAL EXPERIMENTAL PROCEDURES

Automated image processing

Cell segmentation and extraction of raw features

The nuclei channel was used to segment cells (Figure 2A). Individual cells or cell clusters were first detected using the "à trous" wavelet transform. Cell clusters were separated by watershed segmentation in wavelet maps where seeds are initiated on local maxima (Figure 2B and C). Circular regions of 45 microns in radius centered on the nuclei were placed around each nucleus and defined cellular segmentation. To avoid overlapping areas between the circular regions, the regions were cropped appropriately. Since the Golgi falls within the region of segmentation, image features of the Golgi and nucleus within the boundaries of each cell were extracted. Image features that were extracted can be separated into two categories; the first category mainly describes intensities repartition and can be viewed as “generic” features from the field of computer vision while the second category is based on object segmentation and its derived features that are commonly used in quantification of membrane protein localization (Racine et al., 2007).

The first category of image features were composed of intensity average; standard deviation; cumulated intensity; the first 35th Zernike moments; 13 Haralick coefficients (codes adapted from (Boland and Murphy, 2001)); 16 energies in the four wavelet maps after "à trous" wavelet decomposition; calculated on Gabor wavelet decomposition in 8 angles and 8 scales: 8 average of energy over angles, 8 maximum energy over angles and 8 associated angles.

The second category of image features were derived from the segmentation of all bright objects within the cell region and they were composed of descriptors of object segmentation inside cell regions based on "à trous" wavelet decomposition. For each Golgi channel, two sets of segmentations were performed: segmentation of small objects (roughly corresponding to vesicular structures) and segmentation of bigger objects (corresponding to Golgi or Golgi fragment structures). Only the nuclei segmentation was obtained from the nuclei channel. To be independent of intensities, the thresholds are adapted to the intensities of the cells. The threshold value in a wavelet map is proportional to the standard deviation of pixels in the original image that are included in cell regions. Thus the threshold value is independent of the area covered by the cells in the field and is proportional to the cell intensity. 7 segmentations (1 for the nuclei and 2 from each Golgi channel) are obtained in total. These 7 segmentations were described by the number of pixels in the segmentation; the perimeter; the number of objects; percentage of intensity inside the segmentation; the major axis, the minor axis, the angle, the ratio between the minor and the major of an ellipse; fitting is performed on the segmentation; the distance between the region center and the segmentation centroid; the average distance between region center and pixels of the segmentation. We found that image features in the second category were more stable to intensity changes in Golgi channels which, hence, led us to only use image features from the second category to describe the Golgi. Both categories were used to describe the nucleus. A total of 22 features for each of the three Golgi channel and 108 features for the nuclei channel (174 image features in total) were selected to describe the Golgi and nucleus of each imaged cell (Figure 2D).

Cell filtering

A number of cell filtering parameters were adhered. Cells with half nucleus in the image, cells present in a dense cluster, out-of-focus cells (based on nuclei channel), cells displaying the lowest 15% of intensities in each of the Golgi channels per well, and apoptotic and mitotic cells were rejected for further analysis (Figure 2E). A SVM was created to identify out-of-focus cells. Briefly, manual cell scoring of cells in 10 wells was performed to identify the image feature that is most indicative of out-of-focus pattern. Human visualization scored 2000 cells were in focus while 252 cells were out-of-focus. Based on the best z-score to separate the two subpopulations, 'channel[1].Intensities.aTrousDirectional[1].max' image feature was selected for the SVM model. To generate the SVM for apoptotic and mitotic cells, cells with such characteristics were manually identified from 10 wells in 10 different siRNA plates and their nuclei image features were sent to the SVM for learning. The top 5 image features were selected according to their z-scores. We used the radial basis SVM (Fan and Chen, 2005) using the LibSVM implementation. The parameters ‘cost’ and ‘gamma’ are chosen in the interval 2^{-5} to 2^{15} using a modified version of Python script ‘grid.py’ available on the LIBSVM website. The best parameters are ‘cost=2^{11}’ and ‘gamma=2^{-5}’ and lead to an accuracy of 93.0% using a 5-fold cross-validation. The prediction of the classifier was applied to all plates of the screen.

SVM model for generation of phenotypic feature (PF)

Three main classifiers were used to define known phenotypes of the Golgi: diffuse, fragmented and condensed, referred as svm(D), svm(F) and svm(C). (Figure 2F). A cell with a Golgi phenotype similar to control cells will not be assigned a phenotype. For each classifier, different authors visually selected treatments where a majority of cells were clearly attributed to the phenotype. For each “diffuse”, “fragmented” and “condensed” phenotype and each channel, a list of representative treatments were defined for each Golgi channel (Figure S2A). These were compared with untransfected control cells. The 5 most relevant features were selected according to their z-scores to separate the cells that show phenotype versus normal cells (Figure S2D). The three classifiers were calculated via SVM and linear kernel function using the LibLINEAR implementation (Fan et al., 2008). A linear kernel was chosen instead of radial kernel because linear kernels are more stable even if the accuracy is reduced. The linear kernel is more reliable for predicting the major trend of the PF and does not extrapolate the mapping in regions where there are very few cells. In the implementation of each PF SVM training, we chose the same number of cells for both classes (normal and cells with phenotypes) and we attributed a cost to the negative label twice bigger that the positive control one. This unbalancing of the two labels allows more stringency on the affected phenotype (condensed, diffuse or fragmented) than of the normal phenotype. The parameter ‘cost’ is chosen in the interval 2^{-5} to 2^{15} using a modified version of Python script ‘grid.py’ available on the LIBSVM website. We chose the parameter ‘cost=2^{8}’ because it maximizes the accuracy average of the 3 PFs. When a cell shows more than one affected phenotype (like diffuse and fragmented) only the strongest one

is retained by comparing the probability estimates proposed by LibLINEAR (-b option). Genes are represented by the percentage of cells displaying each of the 3 PFs in each of the 3 Golgi channels (Figure 2H). The high-content dataset containing the raw features and SVM phenotypic features on a single-cell level is deposited in the Dryad repository: http://dx.doi.org/10.5061/dryad.1m2p3.

Montage visualisation

We have developed a software dedicated to the visualization of the segmented cells in a montage grid of all four image channels (Figure 2E). This software includes many features for efficient validation of cellular results as different channels can be visualised separately and display colors can be customized.

Validation of phenotypes from SVM prediction

Cell-by-cell validation of Golgi phenotypes: Three users visually scored the golgi phenotypes (three compartments) of 300 cells into 4 categories: “Diffuse”, “Fragmented”, “Condensed”, “Normal”, independently of each other and of the SVM’s prediction. Cells were chosen from 10 wells that exhibit varying weak SVM-predicted phenotypes. The percentages of cells for which the phenotype predicted by the SVM is in agreement with the user’s classification and for which there was inter-user agreement were calculated and categorised as “Complete”, “Moderate” or “Weak” agreement. “Complete” agreement occurs when both the user and SVM/other user attributes the same phenotypic classification to a cell. “Moderate” agreement occurs when a user interprets a phenotype in the cells while the SVM/other user identifies it as “normal” or

vice versa. “Weak” agreement occurs when a user selects a phenotype other than the phenotype classified by the SVM/other user or vice versa.

Validation at the well-level: Images from 120 wells were chosen randomly, among which 20% were from untreated wells and 80% from siRNA-treated wells. Two users visually classified the general phenotype in each well in a blind manner. The percentage of wells where there was agreement between the user and SVM output was calculated and categorized as above.

Validation of lectin specificities

PNA and HPL: Peanut Agglutinin and *Helix Pomatia* lectin and are highly specific for O-glycans, PNA recognizing terminal core 1 O-glycans (Swamy et al., 1991) and HPL terminal α-linked O-GalNAc. KD of C1GALT1, the Core 1 galactosyltransferase that generates the Gal-β1,3-GalNAc-α1-Ser/Thr (T antigen) structure that PNA recognizes, abolishes the already-low PNA staining while increasing HPL staining because of the increase in terminal O-GalNAc. ConA: Concanavalin A binds mainly α-D-mannosyl and α-D-glucosyl groups, having a high affinity for the N-glycan trimannosyl core, thus it tends to reveal high mannose N-glycans (Debray et al., 1981). To test its binding specificity, we knocked down MGAT1 (mannosyl α1,3-glycoprotein β1,2-N-acetylglucosaminyltransferase) which transfers the first GlcNAc residue onto the mannosyl core of N-glycans and is thus essential for the conversion of high-mannose to hybrid and complex N-glycans. Its absence prevents further trimming of the oligomannose structure, promoting more high-mannose glycan structures, and its KD indeed increased ConA staining relative to a GFP KD control. LCA: Lens culinaris agglutinin-A has high affinity for Fuc-α1,6-GlcNAc-N-Asn containing N-glycans (Debray

et al., 1981). As a control, we knocked down FUT8 (fucosyl transferase 8) which catalyzes the addition of fucose in α1,6 linkage to the first, Asn-linked GlcNAc residue of N-glycans. Its absence prevents the formation of this core fucose structure and its KD indeed decreased LCA staining. PHA-L: *Phaseolus vulgaris* leucoagglutinin has specificity for tri- and tetra-antennary N-glycans, binding preferentially to GlcNAc in a β1,6 linkage with the trimannosyl core (Schwarz et al., 1996; Cummings and Kornfeld, 1982). To impair N-glycan synthesis, we co-knocked down STT3A and STT3B, subunits of the oligosaccharyltransferase complex which initiates N-glycosylation by catalyzing the transfer of a lipid-linked high mannose oligosaccharide to an asparagine residue on nascent polypeptide chains, and the KD inhibits PHA-L binding. ECA: *Erythrina cristagalli* lectin has a preference for the disaccharide galactosyl-β1,4-N-acetylglucosamine, therefore recognizing mostly extended complex N- and O-glycans that are not capped by a sialic acid (Kaladas et al., 1982). KD of SLC35A3 (Golgi UDP-GlcNAc transporter) reduces the availability of UDP-GlcNAc substrate necessary for the addition of GlcNAc to extend both N- and O-glycans; KD of MGAT1 or C1GalT1 inhibits the extension of N-glycans or O-glycans, respectively, and thus Gal-β1,4-GlcNAc structures. Thus KD of either of the three genes all lead to a reduction in ECA staining. DSL*: Datura stramonium* lectin has a relatively broad specificity for poly-LacNAc-extended N-and O-glycans as well as tri- and tetra-antennary N-glycans (Sun et al., 2009; Crowley et al., 1984; Cummings and Kornfeld, 1984). Like PHA-L, co-KD of STT3A and STT3B decreases the initiation of N-glycosylation which hence inhibits DSL binding. MAL-II: Maackia amurensis lectin II binds preferentially to O-linked glycans

containing the trisaccharide Sia-α2,3-Gal-β1,3-GalNAc (Geisler and Jarvis, 2011). Sialidase treatment reduces MAL-II staining.

Kinase inhibitor treatment

All kinase inhibitors IPA3 (#3622), FR180204 (#3706) and SP600125 (#1496) were purchased from Tocris Bioscience and reconstituted in DMSO. 3 days after siRNA transfection, cells were treated with various concentrations of the inhibitors for 6 hours before paraformaldehyde fixation.

Western blot analysis

Wild type Hela cells were transfected with siRNAs in a 10cm dish for 3 days. On the third day, Cells were washed twice using ice-cold D-PBS before scraping in D-PBS. Cells were centrifuged at 300g for 5 min at 4°C and were lysed with ice-cold lysis buffer (50 mM Tris [pH 8.0, 4°C], 200 mM NaCl, 0.5% NP-40 alternative, 1 mM DTT, and complete protease inhibitor [Roche]) for 30 min with gradual agitation before clarification of samples by centrifugation at 10,000 g for 10 min at 4°C. Samples were diluted in lysis buffer with 4x SDS loading buffer and boiling at 95°C for 2 min. They were then resolved by SDS-PAGE electrophoresis using bis-tris NuPage gels as per manufacturer's instructions (Invitrogen) and transferred to PVDF membranes which was blocked using 3% BSA dissolved in TBST (50 mM Tris [pH 8.0, 4°C], 150 mM NaCl, and 0.1% Tween 20) for 2 h at room temperature. Membranes were washed to remove traces of BSA before incubation with antibodies as per manufacturer's instructions. Membranes were washed five times with TBST before incubation with secondary HRP-

conjugated antibodies (GE Healthcare). Membranes were further washed five times with TBST before ECL exposure.

Secondary Met-Luc secretion screen

HeLa cells were stably transfected to express secreted *Metridia* Luciferase (Clontech) using lentivirus transduction (HeLa Met-Luc). siRNA transfection of HeLa Met-Luc cells was performed as in the primary screen. After 3 days, the cells were washed once with PBS and fresh media was added to allow Met-Luc secretion. In some wells without siRNA KD, media containing either 10 µg/ml BFA, 6 µg/ml nocodazole, 1 µg/ml monensin, or 1 µg/ml latrunculin B was added instead. 25ul of supernatant per well was extracted after 4 hours, and the amount of secreted Met-Luc quantified using the Ready-to-Glow secreted luciferase reporter assay (Clontech). The raw signals were divided by the cell number (quantified by DAPI staining and imaging), logged, and then normalized to the mean of the control transfection reagent-treated (TR) wells. We used the standard deviation (SD) of TR wells as a measure of assay variation, and defined significant perturbation of Met-Luc secretion as a deviation of more than 3 SDs from the TR mean. This corresponded to normalized secretion values of about 0.95 and 1.05 (see Figure S8).

VSVG Secretion assay

HeLa cells were stably transfected to express the temperature sensitive mutant of VSVG protein (VSVG-tsO45) tagged with mcherry at the C-terminus. siRNA transfection of HeLa-VSVG cells was performed as in the primary screen. Two days after siRNA

transfection, the cells were transferred to 40ºC and incubated for 16 hours to allow accumulation of VSVG in the ER. The cells were then incubated at 32ºC for 15 mins in the presence of 100 µg/ml of cycloheximide before fixation.

SUPPLEMENTAL REFERENCES

Boland, M. V., and Murphy, R. F. (2001). A neural network classifier capable of recognizing the patterns of all major subcellular structures in fluorescence microscope images of HeLa cells. Bioinformatics *17*, 1213–1223.

Crowley, J. F., Goldstein, I. J., Arnarp, J., and Lönngren, J. (1984). Carbohydrate binding studies on the lectin from Datura stramonium seeds. Arch. Biochem. Biophys. *231*, 524–533.

Cummings, R. D., and Kornfeld, S. (1982). Characterization of the structural determinants required for the high affinity interaction of asparagine-linked oligosaccharides with immobilized Phaseolus vulgaris leukoagglutinating and erythroagglutinating lectins. J. Biol. Chem. *257*, 11230–11234.

Cummings, R. D., and Kornfeld, S. (1984). The distribution of repeating [Gal beta 1,4GlcNAc beta 1,3] sequences in asparagine-linked oligosaccharides of the mouse lymphoma cell lines BW5147 and PHAR 2.1. J. Biol. Chem. *259*, 6253–6260.

Debray, H., Decout, D., Strecker, G., Spik, G., and Montreuil, J. (1981). Specificity of twelve lectins towards oligosaccharides and glycopeptides related to N-glycosylproteins. Eur. J. Biochem. *117*, 41–55.

Fan, R., Chang, K., and Hsieh, C. (2008). LIBLINEAR: A library for large linear classification. The Journal of Machine ….

Fan, R., and Chen, P. (2005). Working set selection using second order information for training support vector machines. The Journal of Machine Learning ….

Geisler, C., and Jarvis, D. L. (2011). Effective glycoanalysis with Maackia amurensis lectins requires a clear understanding of their binding specificities. Glycobiology *21*, 988–993.

Kaladas, P. M., Kabat, E. A., Iglesias, J. L., Lis, H., and Sharon, N. (1982). Immunochemical studies on the combining site of the D-galactose/N-acetyl-D-galactosamine specific lectin from Erythrina cristagalli seeds. Arch. Biochem. Biophys. *217*, 624–637.

Racine, V., Sachse, M., Salamero, J., Fraisier, V., Trubuil, A., and Sibarita, J.-B. (2007). Visualization and quantification of vesicle trafficking on a three-dimensional cytoskeleton network in living cells. J Microsc *225*, 214–228.

Schwarz, R. E., Wojciechowicz, D. C., Park, P. Y., and Paty, P. B. (1996). Phytohemagglutinin-L (PHA-L) lectin surface binding of N-linked beta 1-6 carbohydrate and its relationship to activated mutant ras in human pancreatic cancer cell lines. Cancer Lett. *107*, 285–291.

Sun, Q., Kang, X., Zhang, Y., Zhou, H., Dai, Z., Lu, W., Zhou, X., Liu, X., Yang, P., and Liu, Y. (2009). DSA affinity glycoproteome of human liver tissue. Arch. Biochem. Biophys. *484*, 24–29.

Swamy, M. J., Gupta, D., Mahanta, S. K., and Surolia, A. (1991). Further characterization of the saccharide specificity of peanut (Arachis hypogaea) agglutinin. Carbohydrate Research *213*, 59–67.